PERGAMON

International Journal of Heat and Mass Transfer 42 (1999) 2071–2083

International Journal of HEAT and MASS TRANSFER

Measurements of heat transfer and fluid flow in a rectangular duct with alternate attached–detached rib-arrays

J.P. Tsia, J.J. Hwang*

Department of Mechanical Engineering, Chung-Hua University, Hsinchu 300, Taiwan

Received 20 February 1998

Abstract

Experiments are conducted to study the heat transfer and friction in a rectangular duct roughened by arrays of alternate attached and detached ribs. The Reynolds number Re based on duct hydraulic diameter ranges from 12 000 to 70 000, whereas the rib pitch-to-height ratio (P_i/h) varies from 10 to 30. The rib to channel height ratio and the ratio of the rib clearance to height are fixed at $h/2B = 0.2$ and $c/h = 0.5$, respectively. Results show that the entrance distance for the composite ribbed duct is longer than that for the fully-attached and detached ribbed ducts. The composition ribbed wall yields the highest fully developed heat transfer coefficient, and moderate pressure-drop penalty among the three types of ribbed walls. Performance evaluation under the constant pumping-power constraint reveals that the composite-ribbed duct performs best of the three ribbed configurations. Semi-empirical correlations for friction and heat transfer in composite-ribbed ducts are developed to account for rib spacing and flow Reynolds number.

Nomenclature

A_p heat transfer surface area of the ribbed duct
B half-height of the duct
c detached rib clearance, see Fig. 1
c_p specific heat at constant pressure
D_e hydraulic diameter. $4B/(1+B/W)$
f Darcy friction factor
f_s friction factor for the smooth duct
G roughness heat transfer function
h rib height
h^+ roughness height, $(h/De)Re(f/8)^{0.5}$
k_f air thermal conductivity
k_w wood thermal conductivity
ΔL channel length for fully developed pressure drop
$\underline{Nu}$ local center-line Nusselt number
Nu_p average center-line Nusselt number for the fully developed ribbed duct flow
Nu_s average Nusselt number for the smooth duct flow
P_i rib pitch
Pr Prandtl number
ΔP pressure drop across the fully developed test section
Q_c net heat transfer rate
R friction roughness function
Re Reynolds number, $U_{ref}D_e/\nu$
St Stanton number, $\overline{Nu}_p/(PrRe)$
T_b local bulk mean temperature of air
T_w local wall temperature
U streamwise mean velocity
U_{ref} channel average velocity
u' streamwise fluctuating velocity
W half-width of the duct
X axial coordinate ($X = 0$ at the duct inlet)
Y transverse coordinate, see Fig. 2
Z spanwise coordinate, see Fig. 2.

Greek symbols
ρ air density
ν air kinematic viscosity.

Subscripts
b bulk mean
N rib index
s smooth
w wall.

Superscript
– average.

* Corresponding author. Tel.: 00 886 35374281; fax: 00 886 35373771; e-mail: jjhwang@chu.edu.tw

0017–9310/99/$ - see front matter
PII: S0017–9310(98)00300–7

1. Introduction

Roughness elements or turbulence promoters have been widely used to enhance heat transfer in various heat exchangers. In the past two decades, heat transfer and friction in ducts with rib-turbulators attached on the walls have been studied extensively. The effects of rib height, rib spacing, rib shape, and rib angle orientation on the heat transfer coefficient and friction factor over a wide range of Reynolds number have been well established [1–13]. Some investigations have been toward lifting the ribs from the heat transfer surfaces with a clearance [14–17]. Local heat transfer on the smooth surface is enhanced due to the acceleration flow through the gap and vortex turbulence after the rib. However, due to lack of fin effect (or rib conduction effect), the increment in overall heat transfer may be insignificant as compared with that of the fully-attached ribbed wall. Consequently, as shown in Fig. 1, the concept of a composite ribbed wall, i.e., attached ribs and detached ribs alternately, is examined in the present work for checking whether it can perform better than the surface roughened only with single type of ribs (i.e., the fully-attached ribbed wall or fully-detached ribbed wall).

Detaching ribs from the wall between any adjacent attached rib will induce vortices around and after the detached ribs. This may greatly enhance the heat transfer on the flat wall portion beneath and after the detached ribs as well as the downstream attached ribs. Moreover, the attached ribs between any adjacent detached rib act not only as turbulators to promote the wall turbulence, but also conductive fins to remove convectively excess heat to the coolant. Therefore, the wall with the combined attached and detached rib roughness may produce even higher heat transfer than that with the attached or detached ribs only.

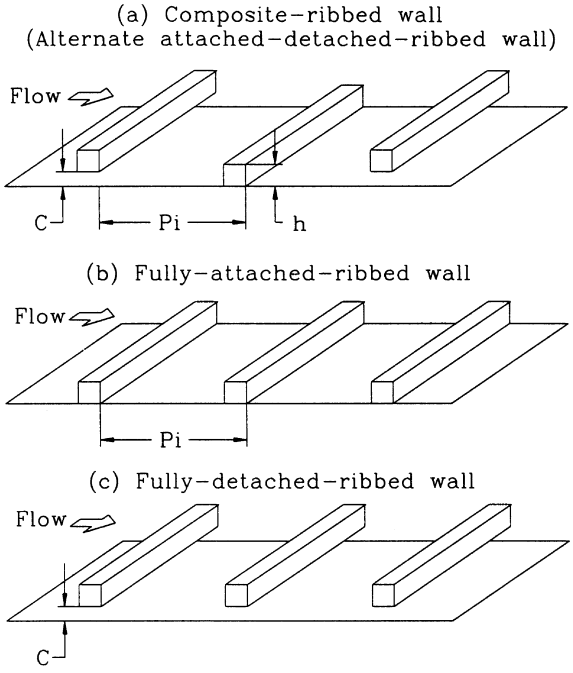

Fig. 1. Typical rib-roughened walls investigated.

Some relevant works concerning the turbulent fluid flow and heat transfer in ducts/pipes with fully-attached and/or fully-detached rib arrays are briefly reviewed below. Burggraf [1] studied the turbulent air flow in a square duct ($W/B = 1$) with transverse ribs ($\alpha = 90^\circ$) attached on two opposite walls for the Reynolds number ranging from 13 000 to 130 000. The average Nusselt number of the ribbed side wall and the friction factor was found to be approximately 2.38 times and 8.6 times, respectively, the corresponding values for fully developed smooth duct flows. Webb et al. [2] presented heat transfer and pressure drop data for fully developed turbulent flow in circular tubes attached internally with transverse square ribs for $0.7 \leqslant Pr \leqslant 37.6$. The geometrical parameters were varied within the ranges of $0.01 \leqslant h/D_e \leqslant 0.04$ and $10 \leqslant P_i/h \leqslant 40$. Correlations for the friction and heat transfer in turbulent tube flow with repeated rib-roughness were successfully developed by taking into account the geometrically non-similar roughness parameter (P_i/h). Later, Gee and Webb [3] studied experimentally the effect of the rib helix angle on turbulent heat transfer and friction for fully developed flow in circular tubes, the helical rib roughness yielded greater heat transfer per unit friction than the transverse rib roughness with the preferred helix angle approximately 49°. Sparrow and Tao [4, 5] systematically investigated the effects of the Reynolds number ($10\,000 \leqslant Re \leqslant 45\,000$), the rib pitch to height ratio ($Pi/h = 9.15$, 18.3 and 36.6), and the rib to duct height ratio ($h/2B = 0.082$ and 0.164) on the mass transfer coefficient and the friction factor for developing duct flows with rod ribs attached both on two opposite walls and on one wall only. The mass transfer number (Sh) was determined by using the naphthalene sublimation technique, but metallic rib-turbulators were not coated with naphthalene, and therefore, the contribution of additional surface area due to the presence of circular rods to heat transfer enhancement was not considered. Han [6] conducted experiments to examine the effect of the duct aspect ratio ($W/B = 1/4$, 1/2, 1, 2 and 4) on the distributions of local heat transfer coefficient in rectangular ducts with two opposite attached ribbed walls for developing turbulent flows under sudden entrance conditions. The local Nusselt number distributions became uniformly periodic between ribs in the axial direction at about $X/D_e \geqslant 3$. Molki and Mostoufizadeh [7] employed the naphthalene sublimation technique for the study of turbulent heat (mass) transfer in rectangular ducts with staggered baffle blockages attached on two

opposite walls. The baffle surfaces were also not covered with naphthalene. Metzger et al. [8] experimentally studied the local convection heat transfer characteristics in square cross-sectional ducts containing attached ribs set at various angles and orientations to produce single- and double-cell secondary flows superimposed on the main streamwise flow. Local heat transfer was determined with a coating material that melted at 43°C. Superior heat transfer performance under the constraint of constant mass flow rate were associated with rib patterns producing a two-cell secondary flow and the significantly superior performance of the 60°, two-cell pattern.

The turbulent heat transfer for fully-detached ribbed duct flows has not been investigated to the same extent as that of the fully-attached ribbed duct flows. Kawaguchi et al. [14] conducted an experiment to investigate the heat transfer characteristics in a rectangular duct with an array of cylinders located near the wall. It was found that during the range of cylinder pitch to diameter ratio (p_i/h = 6.25, 12, 25, 50, ∞) investigated, the values of 12.5 and 25 are recommended for the heat transfer augmentation. Oyakawa et al. [15] examined the effects of geometric shape and of clearance over the two opposite duct walls in a staggered manner on the heat transfer characteristics. The roles of the von Karman vortex shedding and reattachment were documented in detail. Yao et al. [16] investigated local as well as average heat transfer coefficients along a rectangular duct with an array of cylinders staggered over opposite duct walls, the hydrodynamic and thermal fully-developed states were found being started from the fourth array of cylinders, the averaged Nusselt number was achieved more than three times larger relative to smooth duct flow. Liou and Wang [17] investigated the thermal performance enhancement in a rectangular duct with an array of square ribs detached from the duct wall with a fixed rib clearance to height ratio ($c/h = 0.58$) by using holographic interferometry. The local heat transfer deterioration, occurring behind the attached ribs, has been effectively removed by lifting the ribs from the wall with a clearance; the thermally and hydrodynamically developing length for the detached ribbed duct was about three times the duct hydraulic diameter.

The main objective of the present study is to investigate the effect the composite rib-turbulators on heat transfer and pressure drop characteristics in rectangular ducts. Comparisons of the heat transfer/pumping power performance are made among the three novel ribbed geometries given in Fig. 1. Detailed measurements of the flow properties including velocity and turbulence intensity distributions are also investigated for the assistance of understanding the mechanisms of heat transfer augmentation. Moreover, two components that contribute to the heat transfer augmentation, i.e., additional heat transfer surface area, and improved turbulent mixing, are intentionally separated by examining the effect of rib conductivity on the heat transfer for the fully-attached and fully-detached ribbed walls. Some previous plausible findings are also clarified in the present study.

2. Experimental program and data analysis

2.1. Experimental apparatus

Figure 2 shows the airflow system and experimental apparatus employed. It is operated in suction mode and oriented horizontally. From the temperature controlled room, air is pulled into the test section through a sharp-edge entrance, and then, is ducted through a flow meter to a blower. The test duct is 150 cm long, with a rectangular cross section of 160 mm ($2W$) by 40 mm ($2B$) for a duct aspect ratio (w/B) of 4.0, of which the bottom wall serves as heat transfer surface roughened by a composite ribbed array, while the top and two vertical walls are smooth and thermally insulated. Aluminium bars of square cross section (8 by 8 mm) are attached or detached from the heated wall alternately. The attached ribs are glued uniformly on the heated surface by thermal epoxy, whereas the detached ribs are placed over the heated surface with a clearance (c) of 4 mm, and are screwed tightly from the side walls of the duct. Thermofoil (0.018 mm thick) embedded in double-sided tape is uniformly adhered between the stainless steel sheet and fiberglass board to ensure good contact, and is connected with a dc power supply for controllable electrical heating of the test duct. Seventy-six copper–constantan thermocouples are distributed along the spanwise centerline of the heated plate for wall temperature measurements. In order to check the spanwise temperature uniformity, surface temperatures along the lateral of the heated plate ($Z/W = 0.67$) are also instrumented with 30 thermocouples. In the baseline experiments ($P_i/h = 10$), the duct wall is arranged four thermocouples within every rib pitch, which are located at 2.0, 4.0, 6.0, and 8.0 h downstream of rib rear, respectively. In addition, the top wall of each attached rib and the duct wall beneath each detached rib has two thermocouples, respectively. The thermocouple beads of about 0.15 mm in diameter are embedded flush on the wall to avoid flow disturbance. Two thermocouple ranks (each has five beads) are inserted from the bottom duct wall into the duct flow to measure the bulk mean air temperature entering and leaving the test duct. Temperature signals are transferred to a hybrid recorder for pre-processing and then interfaced to a Pentium computer for the calculation of the non-dimensional parameter. For the measurement of the pressure drop across the fully developed flow, two pressure taps located at $X/D_e = 6$ and 12 are connected to a signal-receiving micro-differential pressure transducer which are subsequently amplified by a conditioner and then recorded in a digital readout.

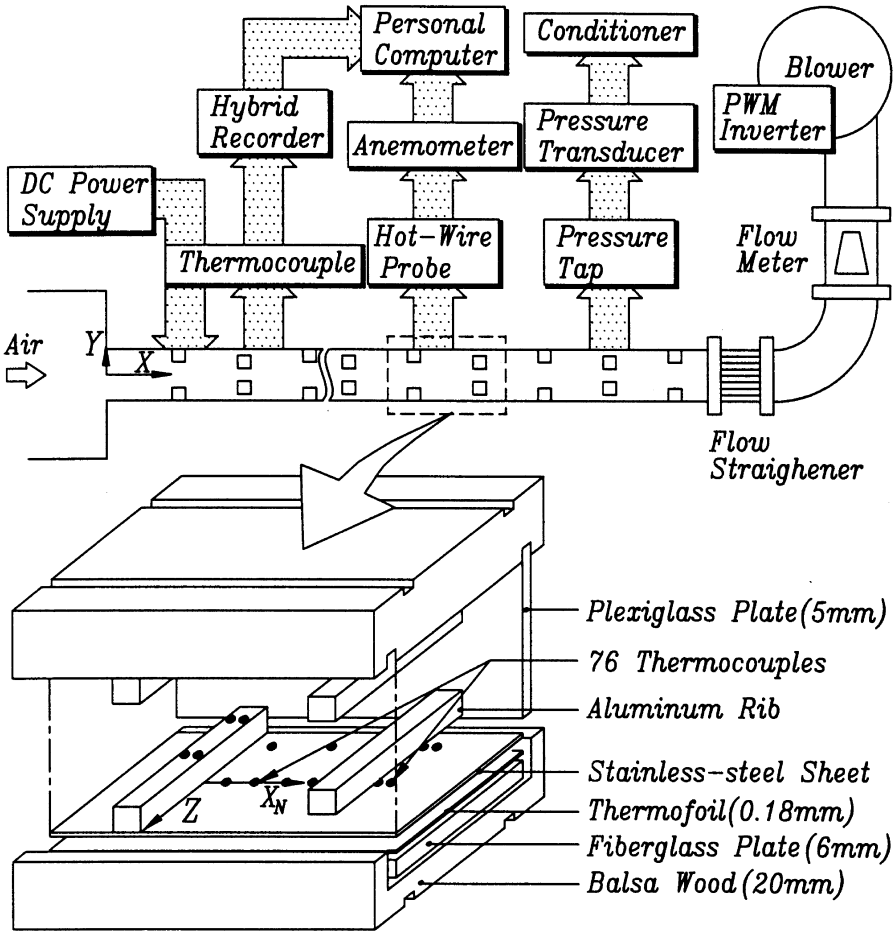

Fig. 2. Sketch of the composite rib-turbulator experimental apparatus, and the construction of the test section.

2.2. Data reduction

The local convection heat transfer coefficient of the heated surface is correlated in terms of the local Nusselt number which is defined as

$$Nu = Q_c D_e/[A_p(T_w - T_b)k_f] \quad (1)$$

Here, Q_c is the net heat transfer rate from the ribbed wall to the coolant, and is calculated by subtracting the heat loss from the supplied electrical power. The electrical power generated from the thermofoil is determined from the measured foil resistance and the current through this foil, and is subsequently checked by measuring voltage drop across each foil. The total heat losses, during the experiment is estimated by:

$$Q_l = Q_{lc} + Q_{lr} \quad (2)$$

Q_{lc} is the conductive heat loss and includes three parts: (1) conductive heat loss from the back side of the heated plate (ribbed wall), (2) conductive heat loss from the two vertical adiabatic plates (smooth walls), and (3) axial conductive heat loss through upstream and downstream ends of the heated plate to the environment. By using the one-dimensional heat conduction analysis, these three conductive losses are estimated to be less than 5.0, 9.0, and 1.0%, respectively, of the total electrical power input for Reynolds number larger than 12 000. The radiative heat loss from the roughened surface to its surroundings, Q_{lr}, is evaluated by a diffuse gray-surface network [18], and is estimated less than 0.5% of the total electrical power input. To confirm the energy conservation in the above calculation, the total net heat transfer rate from the test duct to the cooling air, Q_l, is checked with the enthalpy rise along the test duct.

In equation (1), the local wall temperatures (T_w) are read from the hybrid recorder directly, whereas the local bulk mean air temperatures (T_b) are calculated from the measured duct inlet and outlet air temperature by assuming a linear rise along the test duct. The inlet bulk

mean air temperature is 25–28°C depending on test conditions. The projected surface area of the corresponding ribless wall serves as the heat transfer area (A_p) in equation (1). By using the estimation method of Kline and McClintock [20] the maximum uncertainty of the Nusselt number is less than 8.2% for the case with Reynolds number larger than 12 000. To reduce the influence of Reynolds number on heat transfer augmentation, the local Nusselt number of the present study is normalized by the Nusselt number for fully developed turbulent flow in smooth circular tubes correlated by, the well-known Dittus–Boelter equation as:

$$Nu/\overline{Nu}_s = Nu/(0.023Re^{0.8}Pr^{0.4}) \quad (3)$$

2.3. Friction factor

In fully developed duct flow with mean velocity of air, (U_{ref}), the Darcy friction factor is calculated as:

$$f = (\Delta P/\Delta L)D_e/(\rho U_{ref}{}^2/2) \quad (4)$$

This friction factor is based on adiabatic conditions, i.e. testing without wall heating. Maximum uncertainty of f is estimated to be less than 7.3% for the case of Reynolds number larger than 12 000 by using the uncertainty estimation method of Kline and McClintock [19]. The turbulated rib friction factors are normalized by the friction factors for fully developed turbulent flow in smooth circular tubes proposed by Blasius correlation as

$$f/f_s = f/(0.316Re^{-0.25}) \quad (5)$$

The friction data for turbulent flow in a rectangular duct with two opposite ribbed walls is correlated by modified equations [1, 18]:

$$R(h^+) = (f/8)^{-1/2} + 2.5\ln\{(2h/D_e)[2W/(W+B)]\} + 2.5 \quad (6)$$

where h^+ is the dimensionless roughness height and is defined as $(h/D_e)Re(f/8)^{1/2}$. Similarly, heat transfer data for fully developed turbulent flow in a rectangular duct with two opposite ribbed walls is correlated by the following equations [6, 11]

$$G(h^+,Pr) = (f/8)^{1/2}/St + 2.5\ln\{(2h/D_e)[2W/(w+B)]\} + 2.5 \quad (7)$$

3. Results and discussion

3.1. Developing heat transfer coefficient

Figure 3(a), (b) and (c), respectively, show the local heat transfer coefficient distribution along the axial distance of the three types of ribbed walls, i.e., composite ribbed wall, fully-attached ribbed wall, and fully-detached ribbed wall. Previous results for a smooth duct with sharp entrance [10] are also included for comparison. In these figures, the local Nusselt number ratio, normalized by the Dittus and Boelter correlation shown in equation (3), is plotted as a function of the dimensionless coordinate X/h. The rib pitch to height ratio (P_i/h), and rib to channel height ratio ($h/2B$) are fixed at values of 10 and 0.2, respectively. Note that the results of opposite fully-attached ribbed walls [9] have been obtained using interferometry; however, the current measurements of these three ribbed geometries are by the resistance/thermocouple technique.

The local Nusselt numbers along the axial distance of the three ribbed walls are not uniform. Starting with a local maximum at the immediate region of duct inlet, the local Nusselt number ratio decreases along the axial distance, and then approaches a periodic fully developed distribution after several rib pairs from the duct inlet: typically after the fifth, third and third rib pair for the composite, fully-attached, and fully-detached ribbed walls, respectively. Figure 4 shows the conceptual view of the flow patterns around these three types of rib-roughened walls. It is seen that the flow patterns accompanied by the composite ribbed geometry are more complicated than the other two types of ribbed walls, including flow separation from the attached rib, reattachment on the duct wall, vortices shedding from the detached rib and wall jets ejecting from the rib clearance. The more irregular rib geometry apparently produces a more complex turbulent transportation; and, therefore, the heat transfer coefficient requires a longer distance to develop before setting into a periodic pattern.

3.2. Mean streamwise velocity and turbulence intensity

To confirm the above hypothesis, flow characteristics (including streamwise mean velocity and the intensity of the streamwise velocity fluctuations) in the region downstream of six ribs ($N+1$ to $N+6$) are obtained with hot-wire measurements in cold-flow conditions. For these measurements, an I-type hot-wire probe made of tungsten wire with copper plated ends, having an effective length of 1 mm and a diameter of 5 μm is inserted from the top wall into the duct flow. The probe insertion location is at a distance of six rib-heights from each rib rear face (i.e., $X_N = 6h$), where it is believed to be out of the flow reversal [17]. Measured distributions of mean velocity ratio, U/U_{ref}, and the streamwise velocity fluctuation (turbulence intensity), $\sqrt{u'^2}/U_{ref}$, are shown in Fig. 5(a)–(c), where U_{ref} denotes the average streamwise velocity at the spanwise center-plane ($Z = 0$) of the duct. It is observed that the distribution U/U_{ref}, changes significantly after the first rib-pair location to that after of the second rib pair. After the second rib pair, the distribution of U/U_{ref}, appears to be the same for both the fully-attached and fully-detached ribbed ducts, and changes in cyclic manner for the composite ribbed duct. Both these imply that the streamwise mean velocity comes to periodically fully

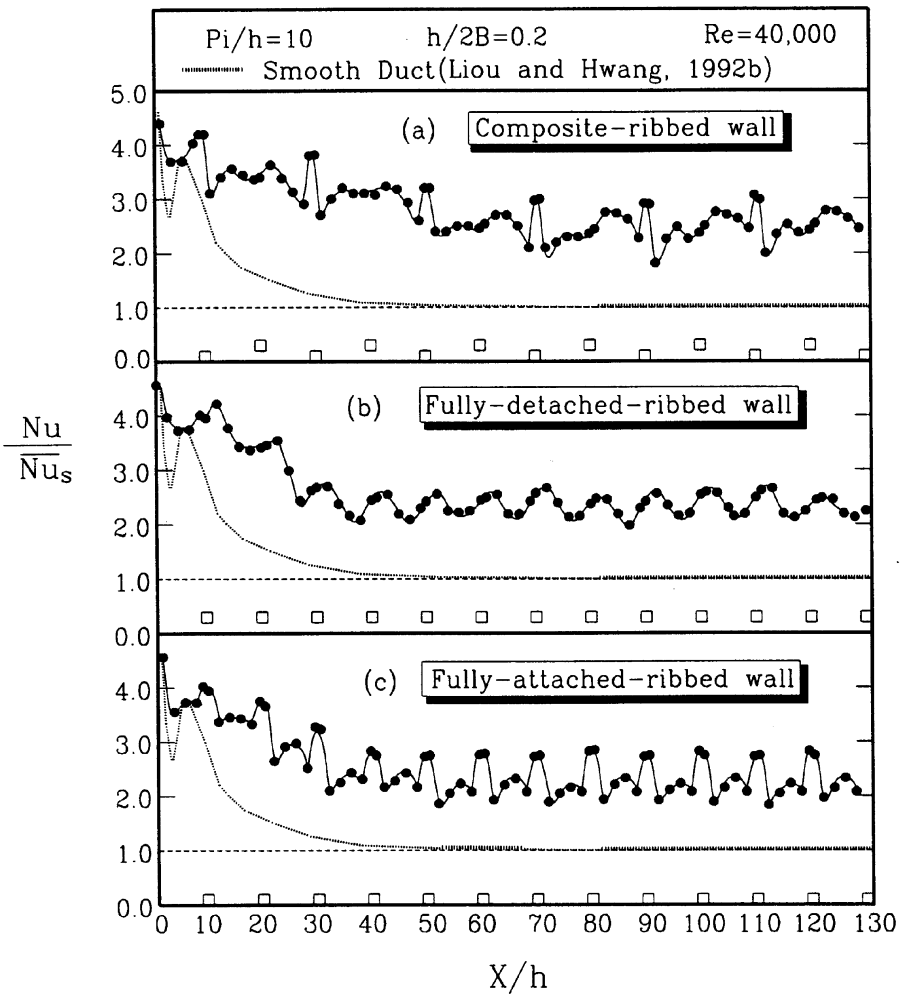

Fig. 3. Local Nusselt number distributions along the axial distance for the three ribbed walls.

developed conditions after the second rib pair for the three ribbed ducts investigated.

For the turbulence intensity distribution, the value of $\sqrt{u'^2}/U_{ref}$ increases rapidly downstream before the third rib pair, especially in the core-flow region. It reaches to an almost identical distribution after the third rib pair for both the fully-attached and fully-detached ribbed ducts, and changes cyclically after the fourth rib pair for the composite-ribbed duct. Consequently, the general conclusion from these figures is that the hydraulically developing length for the composite-ribbed duct is longer than those of the fully-attached and fully-detached ribbed ducts, roughly about four rib pitches distance or five times the duct hydraulic diameter. The longer hydraulically developing length constitutes the above deduction of the more complex turbulent transportation for the composite rib geometry, which is the background for the fully developed thermal field in this duct.

3.3. Average Nusselt number

Figure 6(a) and (b), respectively, show the fully developed average Nusselt number ratio and friction factor ratio for the three types of ribbed walls investigated as a function of Reynolds number. As observed from this figure, the heat transfer augmentation for the composite ribbed wall is in excess of that for the fully-detached and fully-attached ribbed walls with the same rib spacing ($P_i/h = 10$), typically up to 15%. The higher heat transfer coefficient for the duct with composite ribbed walls is, as mentioned before, due to the higher complexity of the turbulent transportation. It is also observed that the Nusselt number ratio decreases with increasing rib pitch to height ratio (P_i/h) for the composite ribbed wall. At the same rib spacing, $P_i/h = 10$, no difference in heat transfer augmentation level, beyond experimental uncertainties, is observed between the fully-attached and fully-detached

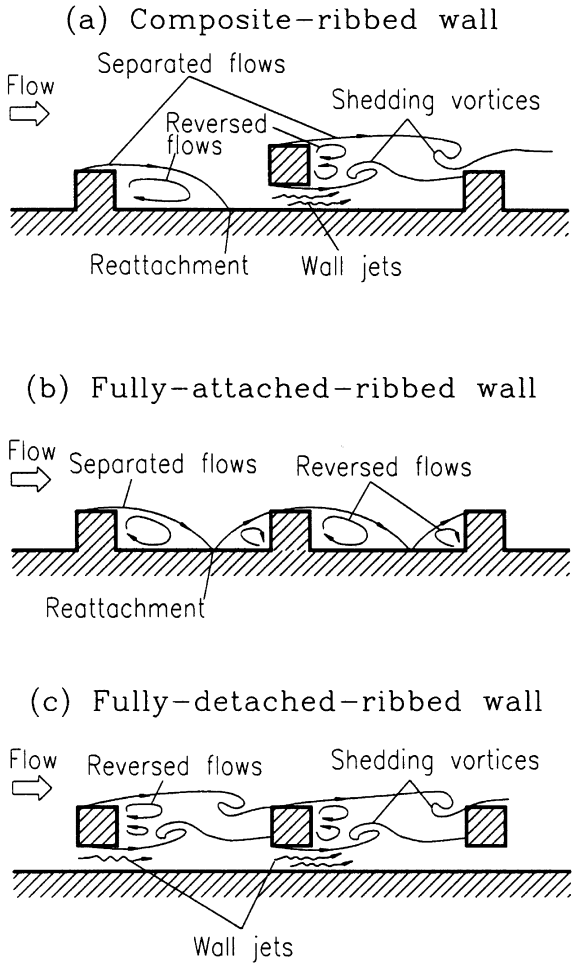

Fig. 4. Conceptual flow patterns in duct with composite, fully-detached and fully-attached ribbed walls.

ribbed walls. A noted trend concluded by the previous work [17] is that the fully-detached ribbed wall (with clearance ratio $c/h = 0.58$) gives about 20–30% higher enhancement in heat transfer as compared with the fully-attached ribbed wall [9] for the same ribbed height [$h/(2B) = 0.13$] and spacing ($P_i/h = 10$). This is not contradictory between the current and these previous results. Note that the average heat transfer coefficient determined in [17] is by integrating the local heat transfer coefficient along the wetting length of the ribbed wall. The average heat transfer coefficient obtained results in difference of the surface area between the fully-attached and fully-detached ribbed walls, over which the average heat transfer coefficient is calculated. That is, the average heat transfer coefficient for the fully-attached ribbed wall is based on the total heat transfer surface area (including two side walls of the rib), whereas that for the fully-detached ribbed wall is based only on smooth duct surface area (ribless wall). Here, in order to place the results on a common basis, the average Nusselt number presented is based on the smooth wall surface area for the three ribbed walls investigated. Consequently, the magnitude of the average Nusselt number obtained by the present work reflects the combined two augmented factors, i.e. the enhanced turbulence mixing by distorting the flow fields caused by the presence of ribs, and the extension in heat transfer surfaces (fin effect) provided by ribs. In fact, if the comparison of the average heat transfer coefficient is made on the same heat transfer surface area as in the previous work, the augmented level in heat transfer for fully-detached and fully-attached ribbed walls should be nearly identical.

3.4. Effect of rib conductivity

It is very instructive to separate the above-mentioned two components that contribute to heat transfer enhancement of the rib-roughened wall, i.e., increase in turbulence mixing, and extension in heat transfer surface area. For this purpose, the effect of the rib conductivity on the average Nusselt number for the fully-detached and fully-attached ribbed walls is examined and shown in Fig. 7. In this study, wood ribs ($k_w = 0.1\ \mathrm{W\,m^{-1}\cdot K^{-1}}$) instead of aluminium bars serves as thermally-nonactive turbulators. There are two trends in this figure can be grouped from the data of the four rib geometries investigated, i.e. the duct with thermally-nonactive ribs attached on the wall (square symbols) provides the worse heat transfer coefficient, whereas the other three augment the heat transfer in almost the same level. Several important conclusions are drawn from this figure. First, because the ribs lifted from the wall with a clearance act as turbulence promoters only, the effect of rib conductivity on the average Nusselt number is ignored. Second, as for the fully-attached ribbed walls, the thermally active rib has a higher average Nusselt number than the thermally-nonactive rib. This implies that the rib conduction (or an increase in surface area) has contributed significantly to heat transfer enhancement for the fully-attached ribbed wall. Third, with regard to the thermally-nonactive ribs, the average Nusselt number for the detached ribs is significantly higher than that for the attached ribs. This signifies that the effect of the enhanced heat transfer through enhancing turbulence is more notable for the fully-detached ribbed wall as compared with that of the fully-attached ribbed wall. However, from the overall average heat transfer comparison the thermally fully-attached ribbed wall is comparable to the fully-detached rib according to Fig. 7.

3.5. Friction factor

Attention is now turning back to Fig. 6(b) for the fully developed friction factor of the three ribbed ducts

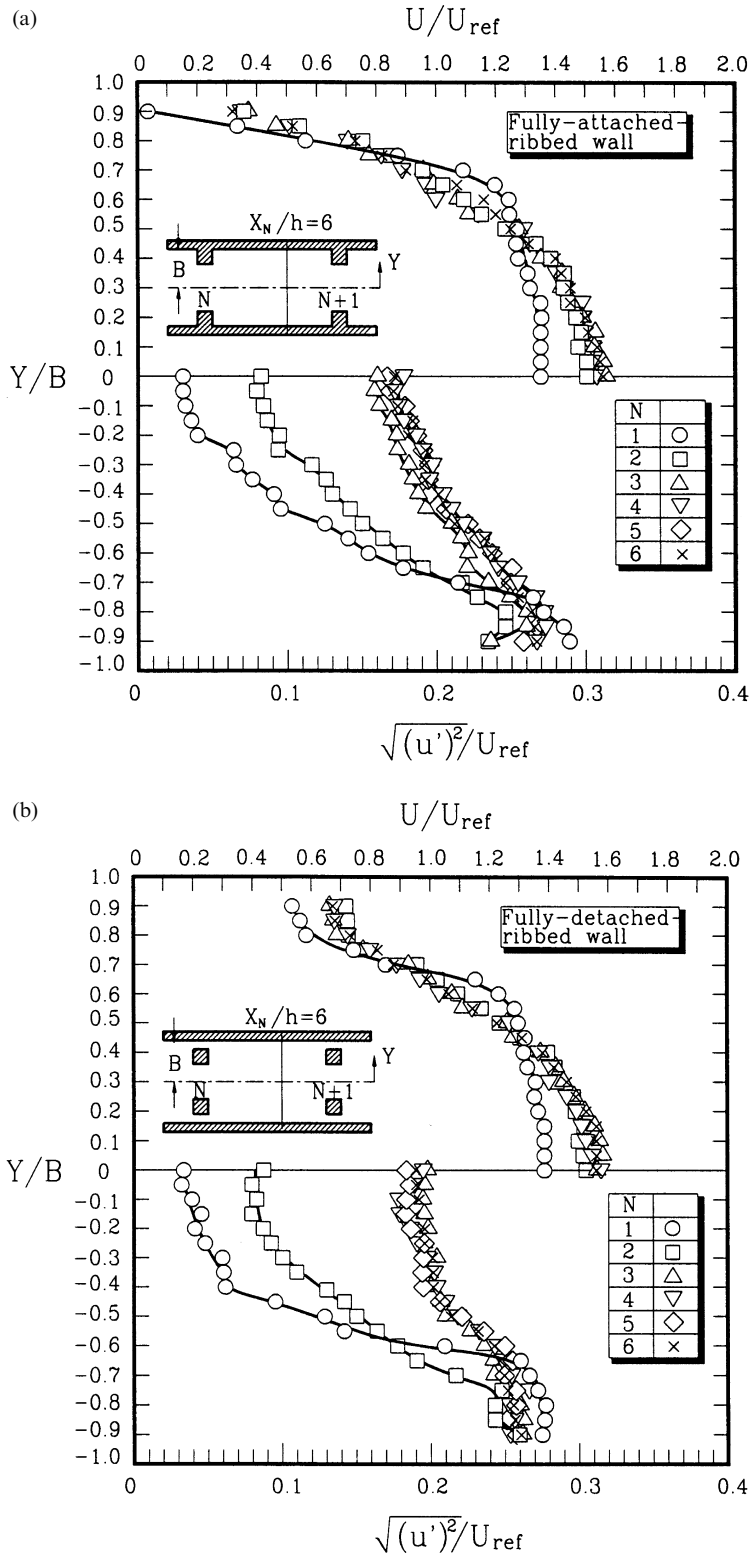

Fig. 5. (a) Streamwise mean and fluctuation velocities at several axial stations of the fully-attached ribbed duct; (b) streamwise mean and fluctuation velocities at several axial stations of the fully-detached ribbed duct; (c) streamwise mean and fluctuation velocities at several axial stations of the composite ribbed duct.

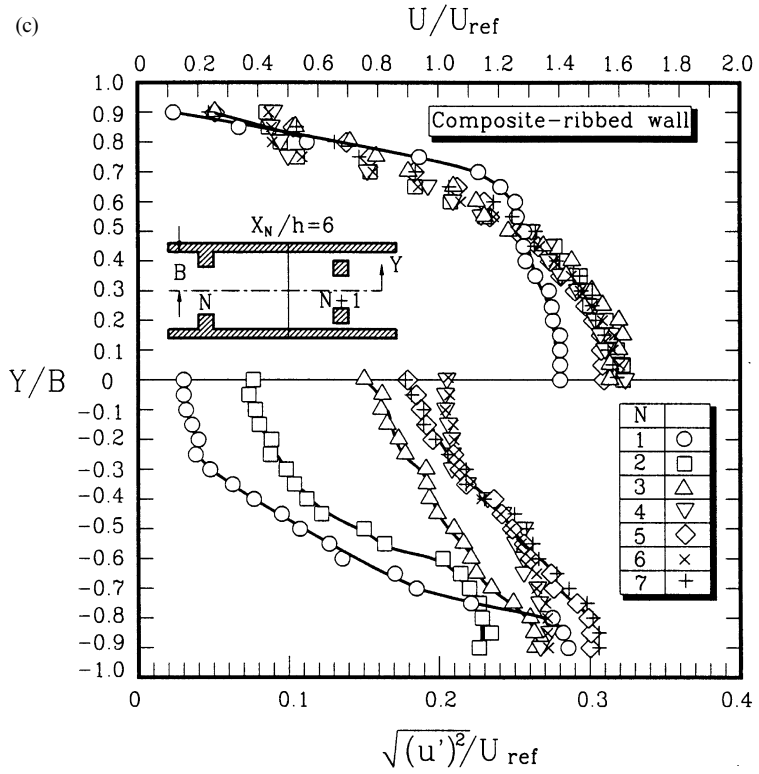

Fig. 5. *Continued.*

investigated. Pressure-drop penalties for the three rib-roughened ducts are roughly the same at the same rib spacing ($P_i/h = 10$), typically about 8–13 times that of the fully developed smooth duct. The friction factor for the fully-detached ribbed duct is slightly higher than the composite ribbed duct, which is slightly lower than the fully-attached ribbed duct. Higher friction factors accompanied by the fully-detached ribbed duct is, with the same form drag (or duct blockage), due to the additional shear flow caused wall jet between rib and duct wall. The friction factor in the composite ribbed duct decreases with increasing rib pitch to height ratio because of less frequency of duct blockages, which is similar to those of the single fully-detached ribbed wall [17] and two opposite fully-attached ribbed walls [9].

3.6. Performance evaluations

In comparing the performance of the ribbed and smooth heat transfer passages, it is necessary to specify the constraints under which the comparison is made. In this work, the comparison of heat transfer performance for the constant airflow rate constraint has already been made in Fig. 6(a) among the three types of rib-roughened ducts. In Fig. 8, the performance comparison is therefore made for the constraint of constant pumping power, which shows the augmented heat transfer per unit pumping power vs flow Reynolds number. It is seen from this figure that the improvement in the Nusselt number ratio of the composite ribbed duct is most prominent among the three ribbed ducts investigated. This is reasonable because of the highest heat transfer enhancement (Fig. 6(a)) and moderate pressure-drop penalty (Fig. 6(b)) for the composite ribbed duct. It is observed that the thermal performance for the fully-attached ribbed duct is nearly the same as the fully-detached ribbed duct at the same rib spacing of $P_i/h = 10$. This is contrary to the conclusion drawn by [17], in which the fully-detached ribbed duct with rib clearance ratio $c/h = 0.58$ performs better than the attached ribbed duct. The inconsistency between the present and these previous results may be due to the following two reasons: first, the difference in the augmented level of heat transfer under equal flow rate constraint exist between this and the previous works, which is due to the aforementioned difference in the definition of average Nusselt number. Second, comparison in the current work is made between the duct with single attached ribbed wall and that with single detached ribbed wall; whereas in Liou and Wang [17], the comparison is made between two ducts with different blockages, i.e. a duct with single detached-ribbed wall and that with two opposite attached-ribbed walls [9]. Figure 8 further shows

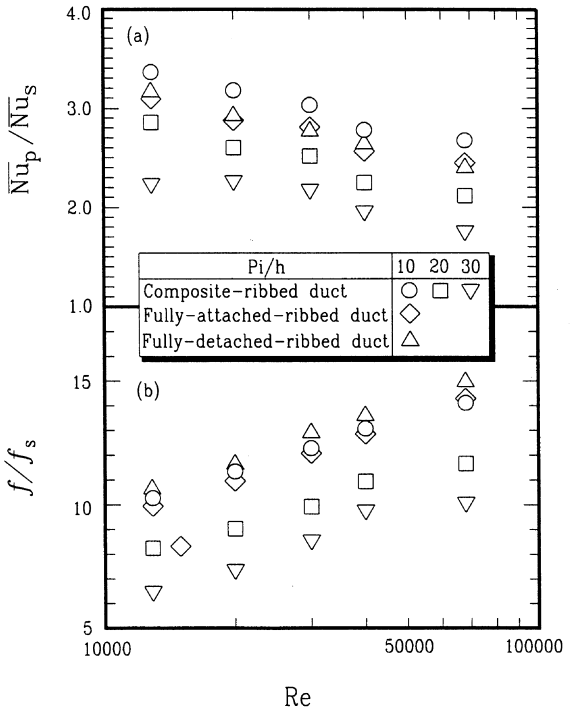

Fig. 6. (a) Average center-line Nusselt number ratio vs Reynolds number; (b) friction factor ratio vs Reynolds number.

that at a lower Reynolds number all of the ribbed ducts perform better than those at higher Reynolds numbers.

3.7. Roughness friction and heat transfer functions

A compact presentation of fully developed heat transfer and pressure drop results can be achieved in terms of the roughness parameters. According to the friction similarity law [2, 6], the measured friction factor, the rib height to channel hydraulic diameter ratio, and Reynolds number could be correlated with the friction roughness function $R(h^+)$. Correlation of the present friction data of the composite ribbed duct shown in Fig. 9 can be expressed in the following form

$$R = 2.9[(P_i/h)/10]^{0.53} \quad (8)$$

The deviation of equation (8) is 8% for 95% of the total data. It is seen from the above equation and Fig. 9 that R is independent of h^+ for all of the ribbed ducts investigated, which means that the effect of the flow Reynolds number on the friction factor is negligible. Figure 9 further shows that previous correlation [2, 20] for the fully-attached ribs in a tube and a rectangular duct is also valid for the present fully-attached ribbed duct. After R is correlated experimentally from equation (8), the friction factor of the present ducts with the composite ribbed walls can be predicted from the combination of equations (6) and (7) for a given h/D_e, P_i/h, W/B, and Re.

Similarly, in accordance with the heat transfer similarity law derived in equation (7), the measured average Stanton number, St, the friction factor, f, and R could be correlated with the heat transfer roughness function $G(h^+, Pr)$. For a Prandtl number of 0.703 in the present study, the correlation for the composite-ribbed duct shown in Fig. 10 can be represented by

$$G = 2.9(h^+)^{0.28}[(P_i/h)/10]^{0.07} \quad (9)$$

The deviation of equation (9) is 8% for 95% of the data shown in Fig. 10 where $(P_i/h/10)^{0.07}$ is neglected. As shown in this figure, again, the previous correlation for the fully-attached ribbed duct [6, 20] is also shown for the prediction of the present data of the fully-attached and fully-detached ribbed ducts.

4. Conclusions

The effect of composite, fully-attached and fully-detached rib-turbulators on friction factors and heat transfer coefficients in rectangular ducts have been examined experimentally. Arrays of alternate attached and detached ribs roughen the duct walls for the composite ribs. The main findings from the experiments are as follows:

(1) The axial distributions of center-line heat transfer coefficients and the profiles of the streamwise mean and fluctuating velocities at several selected axial stations have been obtained for three types of the rib-roughened walls. The thermally and hydrodynamically developing length of the composite rib-roughened wall is longer than those of the fully-attached and fully-detached ribbed ducts, and typically about five rib pitches from the duct inlet.

(2) Fully developed heat transfer coefficients for the composite rib-roughened walls are slightly higher than those for the fully-attached and fully-detached rib-roughened walls with the same rib height and spacing. Among the three ribbed walls investigated, the fully-detached and fully-attached rib-roughened ducts give the highest and lowest pressure drop penalties, respectively. Consequently, the composite ribbed geometry provides superior constant-pumping-power thermal performance than the other two ribbed ones.

(3) The rib conductivity affects significantly on the average heat transfer for the fully-attached ribbed wall, but negligibly for the fully-detached ribbed wall. This implies that the heat transfer augmentation for the attached ribbed wall is contributed not only by the effect of increased turbulence mixing, but also the rib conduction effect (or fin effect); while only the former effect augments the heat transfer for the detached ribbed wall.

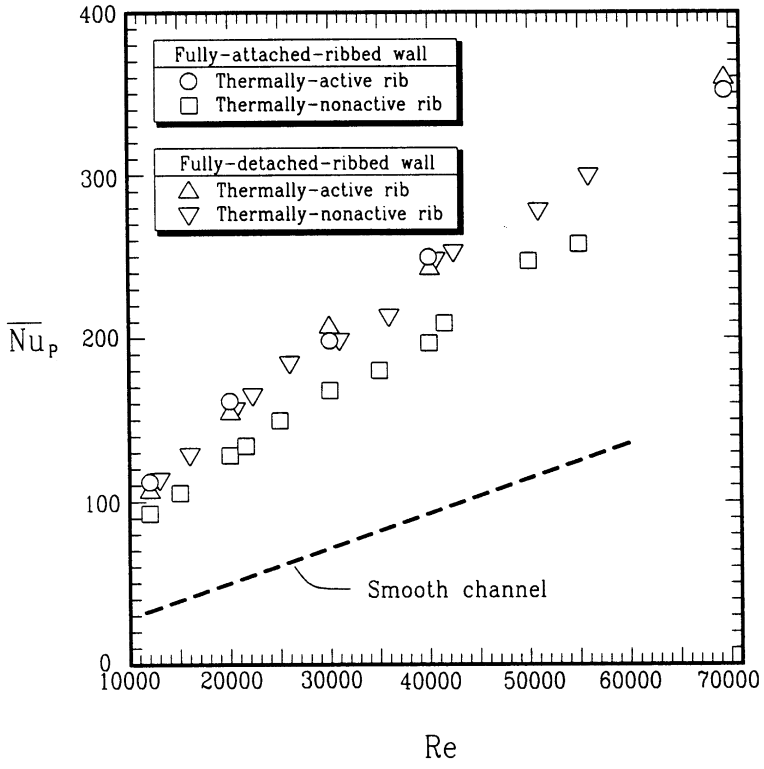

Fig. 7. Effect of the rib conductivity on the average center-line Nusselt number for the fully-attached and fully-detached ribbed walls.

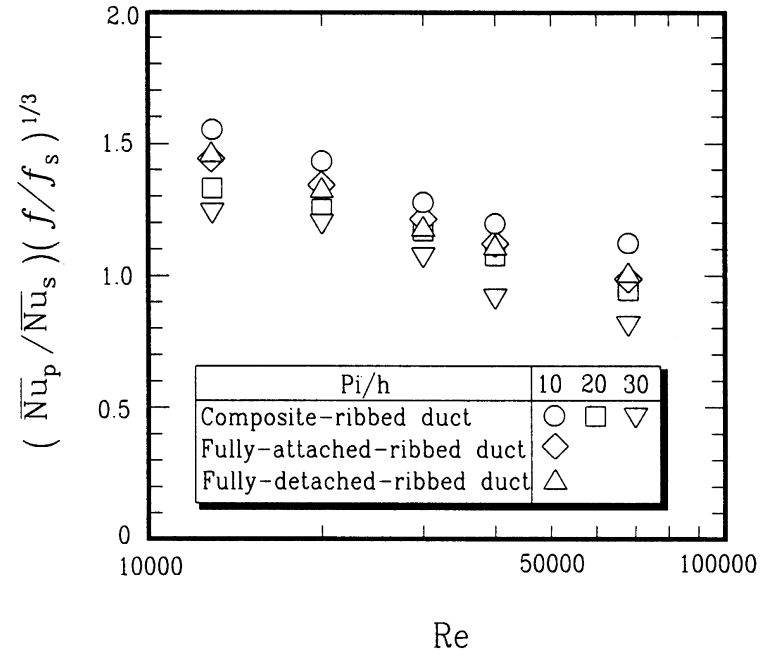

Fig. 8. Performance comparison under the constant pumping power constraint.

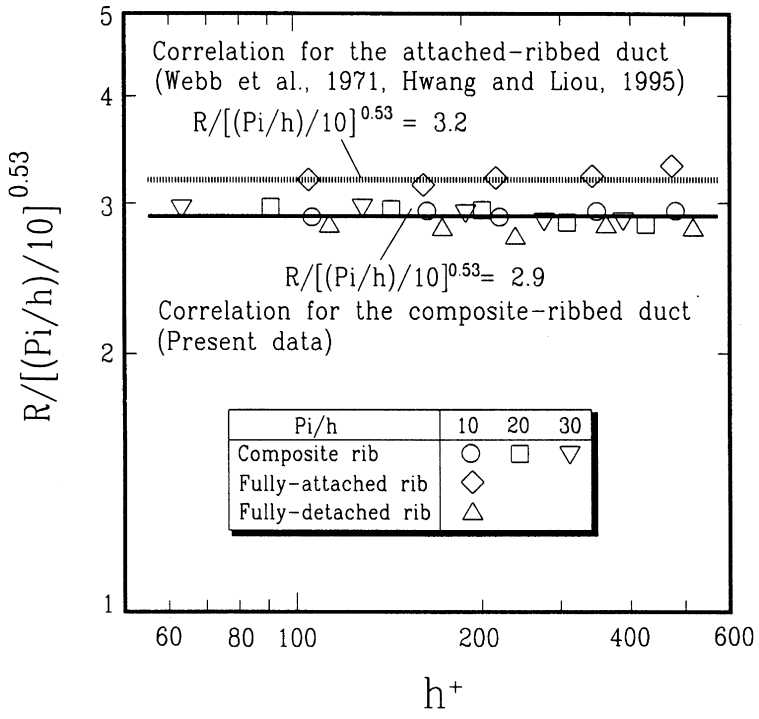

Fig. 9. Roughness friction functions vs roughness height.

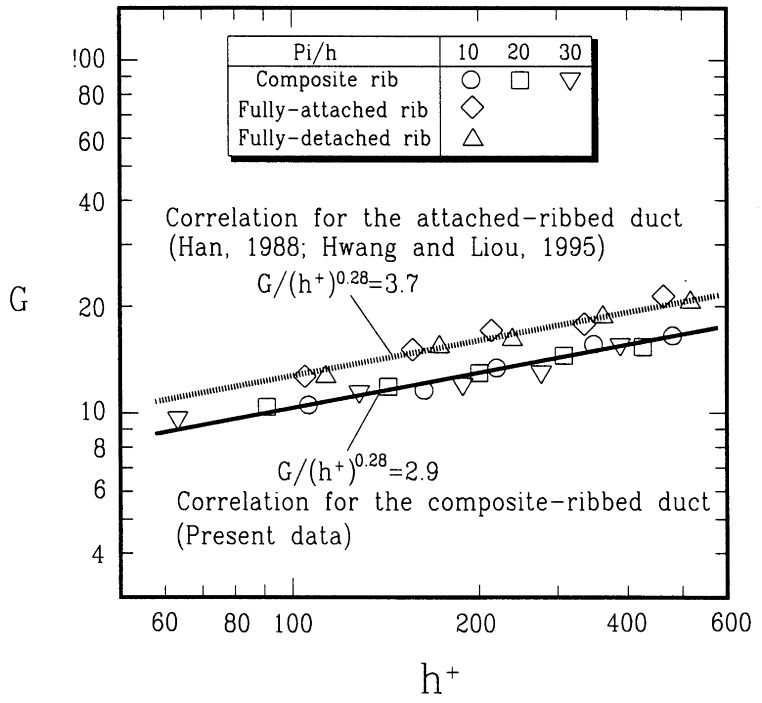

Fig. 10. Roughness heat transfer functions vs roughness height.

(4) A significant disagreement exists in respect of the augmented level in the average Nusselt number for the fully-detached and fully-attached rib-roughened walls between the present work and the test data obtained by laser holographic interferometry in the previous work [17], which is mainly due to the difference in the heat transfer surface area over which the data are calculated. In the present work, to put the results on a common basis, the projected surface area of the corresponding ribless wall serve as the heat transfer area for the average heat transfer coefficients determination; whereas, in the previous work, the average heat transfer coefficients for the fully-attached and fully-detached rib-roughened wall are based on the different heat transfer areas, i.e. total heat transfer surface area (including the rib flank area) and smooth surface area, respectively.

(5) Based on the ribbed duct analysis correlations for roughness friction and heat transfer functions are obtained for the rectangular duct with the composite ribbed wall which has not been reported in the past.

Acknowledgement

Support of this work was provided by the National Science Council under contract number NSC 85-2212-E-216-003.

References

[1] F. Burggraf, Experimental heat transfer and pressure drop with two-dimensional discrete turbulence promoters applied to two opposite walls of a square tube, in: A.E. Bergles, R.L. Webb (Eds.), Augmentation of Convective Heat and Mass Transfer, ASME, New York, 1970, pp. 70–79.

[2] R.L. Webb, E.R.G. Eckert, R.J. Goldstein, Heat transfer and friction in tubes with repeated-rib roughness, Int. J. Heat Mass Transfer 14 (1971) 601–617.

[3] D.L. Gee, R.L. Webb, Forced convection heat transfer in helically rib-roughened tubes, Int. J. Heat Mass Transfer 23 (1980) 1127–1136.

[4] E.M. Sparrow, W.Q. Tao, Enhanced heat transfer in a flat rectangular duct with streamwise-periodic disturbances at one principal wall, Trans. ASME, J. Heat Transfer 105 (1983) 851–861.

[5] E.M. Sparrow, W.Q. Tao, Symmetric vs. asymmetric periodic disturbances at the walls of a heated flow passage, Int. J. Heat Mass Transfer 27 (1984) 2133–2144.

[6] J.C. Han, Heat transfer and friction characteristics in rectangular ducts with rib turbulators, Trans. ASME, J. Heat Transfer 110 (1988) 321–328.

[7] M. Molki, A.R. Mostoufizadeh, Turbulent heat transfer in rectangular ducts with repeated-baffle blockages, Int. J. Heat Mass Transfer 32 (1989) 1491–1499.

[8] D.E. Metzger, C.S. Fan, Y. Yu, Effects of rib angle and orientation on local heat transfer in square ducts with angled roughness ribs, in: Compact Heat Transfer Exchangers: A Festschrift for A.L. London, Hemisphere Publishing Corp., 1990.

[9] T.M. Liou, J.J. Hwang, Turbulent heat transfer augmentation and friction in periodic fully developed duct flows, Trans. ASME, J. Heat Transfer 114 (1992) 56–64.

[10] T.M. Liou, J.J. Hwang, Developing heat transfer and friction in a ribbed rectangular duct with flow separated at inlet, Trans. ASME, J. Heat Transfer 114 (1992) 565–573.

[11] T.M. Liou, J.J. Hwang, Effect of ridge shape on turbulent heat transfer and friction in a rectangular duct, Int. J. Heat Mass Transfer 36 (1993) 931–940.

[12] H.H. Huang, W.Q. Tao, An experimental study on heat/mass transfer and pressure drop characteristics for arrays of nonuniform plate length positioned obliquely to the flow direction, Trans. ASME, J. Heat Transfer 115 (1993) 568–575.

[13] C.M. Ling, Y.Y. Jin, Z.Q. Chen, Heat/mass transfer and pressure drop in triangular-rib-rib-roughened rectangular channel, Int. J. Heat and Fluid Flow 15 (1994) 486–490.

[14] Y. Kawaguchi, K. Suzuki, T. Sato, Heat transfer promotion with a cylinder array located near the wall, Int. J. Heat and Fluid Flow 6 (1985) 249–255.

[15] K. Oyakawa, T. Shinzato, I. Mabuchi, Effect of heat transfer augmentation of some geometric shapes of a turbulence promoter in a rectangular duct, Bull. JSME 29 (1986) 3415–3420.

[16] M. Yao, M. Nakatani, K. Suzuki, An experimental study on pressure drop and heat transfer in a duct with a staggered array of cylinders, Proceedings of ASME–JSME Thermal Engineering Joint Conference 5 (1987) 189–196.

[17] T.M. Liou, W.B. Wang, Laser holographic interferometry study of developing heat transfer in a duct with a detached rib array, Int. J. Heat and Mass Transfer 38 (1995) 91–100.

[18] R. Seigel, J.R. Howell, Thermal Radiation Heat Transfer, 2nd ed., McGraw-Hill, New York, 1981.

[19] S.J. Kline, F.A. McClintock, Describing uncertainties on single-sample experiments, Mechanical Engineering 57 (1953) 3–8.

[20] J.J. Hwang, T.M. Liou, Heat transfer and friction in a low-aspect-ratio rectangular duct with staggered perforated ribs on two opposite walls, Trans. ASME, J. Heat Transfer 117 (1995) 843–850.